Finite deformations of an initially stressed cylindrical shell under internal pressure

Paul Gonçalves, Djenane Pamplona, Stefane Lopes

Finite deformations of an initially stressed cylindrical shell under internal pressure

P.B. Gonçalves, D. Pamplona, S.R.X. Lopes

Civil Engineering Department, Pontifical Catholic University, Rio de Janeiro, Brazil

This paper investigates the large deformations of an extended thick cylindrical tube under internal pressure, with emphasis on the static nonlinear behavior and instabilities of the shell. Thick elastic tubes that undergo large elastic deformations under internal pressure can exhibit novel instabilities. After some deformation, part of the tube becomes highly deformed taking the form of a bulge, while the remainder appears almost unchanged. This local instability phenomenon corresponds to a limit point along the nonlinear equilibrium path. After the onset of these highly nonuniform deformations, the local bulge initially grows with a marked decrease in internal pressure while the rest of the tube unloads. First, a detailed experimental analysis is carried out involving different geometries and initial axial forces and the influence of the axial force and of the internal pressure on the critical pressure is investigated. The shell used in the experiments is composed of an isotropic, homogeneous and hyperelastic rubber, which is modeled as a Mooney–Rivlin incompressible material, described by two elastic constants. These constants are obtained by comparing the experimental and numerical solutions for the shell under axial tension. The governing shell equations are solved numerically using the finite-element method, using the program ABAQUS. The experimental results are, as shown in the paper, in satisfactory agreement with the numerical analysis.

Cylindrical shell; Thick shell; Finite deformations; Hyperelastic material; Local buckling; Large deformations

1. Introduction

Rubber structures are common in several engineering applications and everyone is familiar with some of the physical properties of this class of polymers called elastomers. They are capable of being stretched to several times their original length with relatively small applied forces and, when the force is released, they retract rapidly to the unstressed length with heat transfer on rebound very close to zero. Also, under moderately large deformations, after unloading, they present no permanent deformation as a result of the extension process and, when they are fully elongated, they exhibit very high tensile strength and stiffness. These properties are all observable on the macroscopic level.

The linear constitutive relations valid for the small-strain regime can be sometimes extended to the large displacement small strain case but can lead to unrealistic results when large deformations are present. In such cases, elasticity in the fully nonlinear range must be employed. Seminal contributions in this field include the papers by Rivlin and co-workers [1,2]. His work on the mechanics of rubber (in the 1940s and 1950s) established the basis of finite-elasticity theory. An historical account of large-deformation theory and applications to about 1953 has been given by Truesdell [3]. This has been followed by the classical work of Green and Adkins [4] on nonlinear elasticity. Historically, the large deformations observed in rubber-like materials under several loading conditions motivated researchers over decades to express the associated nonlinear elastic behavior through hyperelastic models [5]. Among the hyperelastic models, strain invariant based Mooney–Rivlin model [6,7] is the oldest one. One of the simplest constitutive models is the neo-Hookean model,

which involves only one elastic constant. Most constitutive relations perform well up to moderate extension range, but cannot represent the strain-hardening behavior typically exhibited by rubbers at very large strain levels [8]. Subsequently, Hart-Smith [9], Alexander [10] and Arruda and Boyce [11], among others, proposed improved models to include a larger class of deformations. Furthermore, stretch-based models such as those proposed by Ogden [12,13] were also formulated.

The analysis of thin hyperelastic cylindrical shells has been a problem of continued interest. The investigation of the equilibrium and stability of thin cylindrical tubes under uniform pressure loading or loads acting along the boundaries has been examined theoretically, for instance, by Corneliussen and Shield [14]; Alexander [15], Haughton and Ogden [16,17]; Ratner [18]; Li and Steigmann [19], Haseganu and Steigmann [20]; Chen [21]; Haughton [22] and Gent [23]. The number of experimental contributions to this class of problems is rather small compared with the theoretical and numerical ones. Among the experimental investigations in this field the publications of Green and Adkins [4], Alexander [15], Pamplona and Bevilacqua [24], Pamplona et al. [25,26] and Vangerko and Treolar [37] should be mentioned. When the thickness of the cylindrical tube is small, it can be modeled as an ideal membrane subjected only to in-plane normal and shearing forces. When the membrane becomes thicker, flexural effects cannot be disregarded in the analysis and the structure must be modeled as a shell or a three-dimensional solid body.

The analysis of large deformations of hyperelastic thick shells is not so common, nevertheless there are some important publications such as the ones by Kyriakides and Chang [27,28] and, more recently, the works by Tang et al. [29] and Haussy and Ganghoffer [30] where the theory of thick hyperelastic shells was used for the modeling of carotid arteries and aneurysms, respectively.

Elastomeric thick shells are load adaptive, as they change their geometry to accommodate external loads with the minimum variation in stress levels, and, therefore, may be an efficient engineering solution in many practical fields. In most of these applications the nonlinearities of deformation and material response are rather important. This work investigates the nonlinear behavior of extended thick cylindrical shells suitably supported, both numerically and experimentally. In the numerical formulation of the problem, the shell material is considered to be incompressible, homogenous, and isotropic and it is modeled as a Mooney–Rivlin incompressible material, described by two elastic constants. This is in agreement with the physical characteristics of the rubber shells used in the experimental investigation. To analyze the large deformations of the tube, elasticity in the fully nonlinear range is considered in terms of a hyperelastic strain potential together with a consistent constitutive law and implemented in a finite-element (FE) code. In the experimental analysis several geometries and loading cases were investigated and these results were compared with the numerical results obtained by using the commercial program ABAQUS [31,32]. This FE code offers a good library of FE and constitutive laws for the large-deformation analysis of shells. This has been here used, together with the Newton–Raphson algorithm and the Riks continuation method, to obtain the pre- and post-bifurcational behavior of the shell under axial tension and internal uniform pressure.

When rubber structures are subjected to certain simple deformations, an unstable condition is reached at a certain critical point. Recently, Gent [8] presented a review of several examples of nonuniform deformations in rubber structures as a result of an inherent elastic instability. Among these problems is the inflation of extended cylindrical tubes under increasing internal pressure. An interesting feature exhibited by inflated thick shells, which can be observed both numerically and experimentally, is the initiation and propagation of localized instability. As the tube is inflated, it first expands radially in a practically uniform manner until a maximum internal pressure is reached. At this limit pressure the cylindrical configuration becomes unstable and a local bulge appear somewhere along the length of the shell. After the onset of buckling, there is a sudden decrease in pressure as the bubble or aneurysm grows, reaching a lower bound at large deflections. This behavior is known in literature as localization [33]. This behavior was first predicted by Mallock [34] and observed in thick hyperelastic membranes by, among others, Kyriakides and Chang [27,28], who analyzed this problem both theoretically and experimentally. In some situations, the tube first presents a global instability mode similar to an Euler column followed by the formation of the local bulge. An analytical solution for this local instability considering thin-walled tubes can be found in Gent [23]. This work is a natural extension to thick shells of the previous paper by the authors on the finite deformations and instabilities of a thin cylindrical membrane under axial tension and internal pressure [26].

2. Problem formulation

2.1. Material identification

Consider a long and thick cylindrical tube of hyperelastic, homogeneous, isotropic and incompressible material (latex). In its undeformed state, the shell has an external radius R, length L and thickness H. The material of this shell is considered to be, based on the experimental results, homogeneous, isotropic and incompressible. The experiments were conducted on commercially available rubber latex tubes. Six shells with different geometries were used. Their geometric characteristics were measured in the Institute of Metrology of the Catholic University (ITUC—PUC-Rio) and the results are presented in Table 1.

Among the more efficient approaches to describe the thermo-dynamical behavior of rubber-like solids are the general concepts of statistical mechanics and the continuum mechanics standpoint, which is phenomenological. Adopting the phenomenological approach, isotropic hyperelastic materials are conveniently represented in terms of a strain energy density w. Assuming the complete recoverability after deformation, the strain energy density depends only on the final state of strain and in no way on the loading history. Thus given an undeformed reference state, the strain is characterized by the principal stretches λ_1, λ_2 and λ_3 or, alternatively, by the strain invariants I_1, I_2 and I_3, that is:

$$w = w(\lambda_1, \lambda_2, \lambda_3) = w(I_1, I_2, I_3). \tag{1}$$

The three strain invariants of the deformation field can be written in terms of the principal stretches λ_i ($i = 1, 2, 3$) as

$$\begin{aligned} I_1 &= \lambda_1^2 + \lambda_2^2 + \lambda_3^2, \\ I_2 &= (\lambda_1\lambda_2)^2 + (\lambda_2\lambda_3)^2 + (\lambda_1\lambda_3)^2, \\ I_3 &= (\lambda_1\lambda_2\lambda_3)^2. \end{aligned} \tag{2}$$

Volume changes in rubber-like materials are very small [35] and the simplifying assumption of incompressibility is usually adopted. Thus the constraint

$$I_3 = 1, \tag{3}$$

Table 1
Shell geometric parameters

Specimen	External radius	Thickness	Length
	R (mm)	H (mm)	L (mm)
B200	2.42	1.22	80
B204	5.90	2.95	324
B205	6.09	2.19	318
B207	6.95	3.13	318
B209	8.36	2.09	318
B210	9.33	3.58	317

is identically satisfied throughout the material. The strain energy density is then considered as a function of I_1 and I_2 only. Hence, the theoretical representation of the behavior of a hyperelastic incompressible material is given by the definition of the function $w(I_1, I_2)$.

There are several constitutive laws in literature particularly adapted to the representation of elastomers. Rivlin [7] has proposed the following polynomial form for the energy density function:

$$w = \sum_{m,n} C_{mn}(I_1 - 3)^m (I_2 - 3)^n, \tag{4}$$

also known as the Mooney–Rivlin strain energy density function because the first order polynomial function

$$w = C_1(I_1 - 3) + C_2(I_2 - 3), \tag{5}$$

has first been introduced by Mooney [6]. Eq. (5) is a function of two constants, C_1 and C_2. This is probably one of the most used densities in FE codes.

A simplified form of Eq. (5)

$$w = C_1(I_1 - 3), \tag{6}$$

known as the neo-Hookean strain density function has also been extensively used in literature.

Another constitutive law used is that due to Ogden [12,13]. In this case the strain energy density function is given by

$$w = \sum_{n=1}^{3} \frac{\mu_n(\lambda_1^{\alpha_n} + \lambda_2^{\alpha_n} + \lambda_3^{\alpha_n} - 3)}{\alpha_n}, \tag{7}$$

where λ_i are the extensions in the principal directions and μ_n and α_n are constants of the material.

The S4R shell quadrilateral, general finite deformation element defined in the ABAQUS menu with four nodes and four integration points was shown to be the best element for this problem and will be used in the present numerical analysis.

In order to establish the shell constitutive law, the shell was first subjected to increasing axial tension loads, as

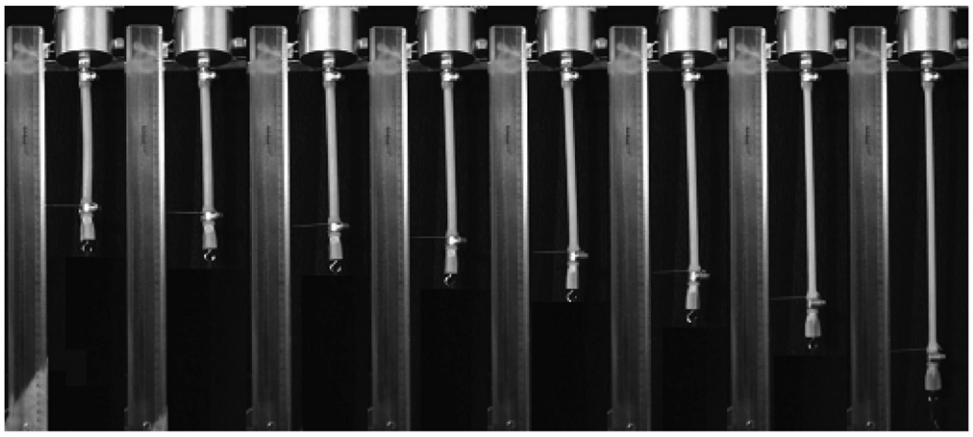

0 N	4.90 N	9.81 N	17.71 N	19.62 N	24.52 N	29.43 N	39.24 N

Fig. 1. Experimental analysis of a thick shell under increasing axial tension. Sequence of photos illustrating a typical test.

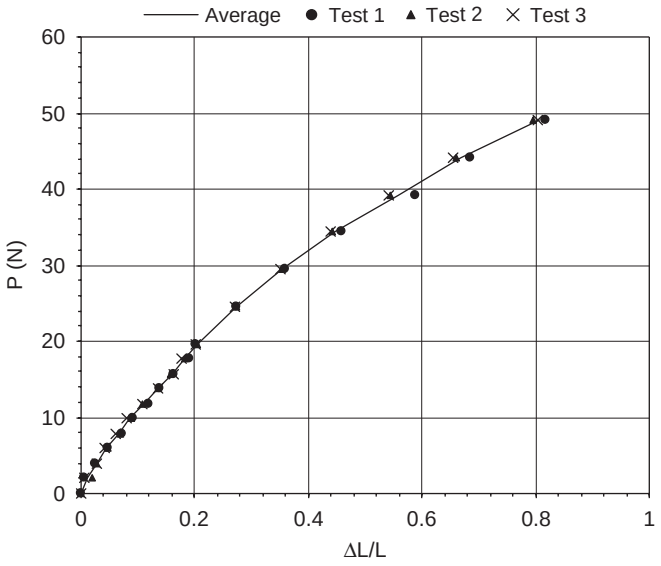

Fig. 2. Experimental results: applied axial load as a function of the nondimensional extension ratio, $\Delta L/L$.

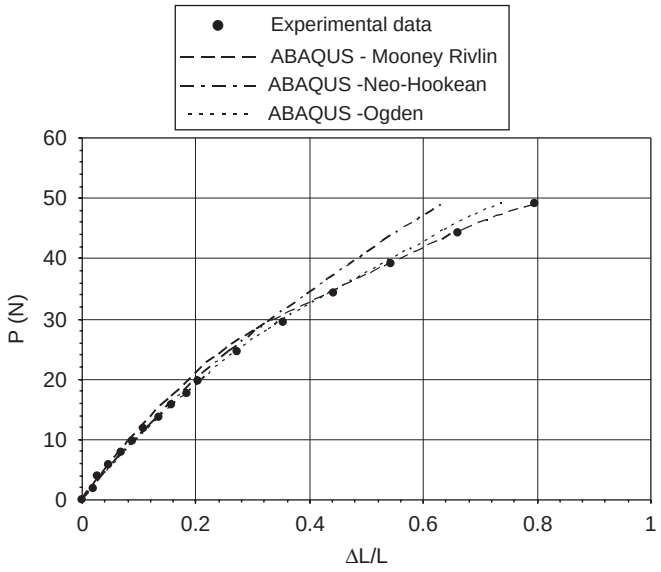

Fig. 3. Comparison of the experimental results for a thick shell under increasing axial tension with the FE results, using three different constitutive laws.

Table 2
Elastic constants of the shell material

Neo-Hookean	$C_1 = 0.201906$ MPa	$C_2 = 0$ MPa
Mooney–Rivlin	$C_1 = 0.087167$ MPa	$C_2 = 0.150843$ MPa
Ogden	$\mu = 1.55886$ MPa	$\alpha = 0.403913$

illustrated in Fig. 1. For each value of the known axial load the relative extension of the shell, $\Delta L/L$, was measured. Here L is the initial length of the shell. The results from three independent analyses are plotted in Fig. 2, together with the average values which are used as the true experimental values to obtain the relevant material elastic constants. As observed here all analyses led to the same nonlinear relation between P and $\Delta L/L$. The same shell under axial tension was analyzed numerically using the software ABAQUS. For this, the S4R shell element, together with the three constitutive laws given in Eqs. (2)–(4), was used and convergence studies were carried out. The final mesh had 2785 elements and 2458 nodes. Using ABAQUS and the experimental results of Fig. 2, the material constants for each constitutive model were calculated using an error minimization procedure and are given in Table 2. This experimental procedure for the determination of the elastic constants had already been used successfully by Pamplona et al. [25] in the analysis of liquid filled membranes. It should be pointed out that this is in fact a biaxial test since the deformations in the two principal directions of the tube are considered.

Finally, using these constants, the load–axial displacement curve for each constitutive law was obtained using the FE program and the results compared with the experimental ones. Good agreement was observed between the experimental and numerical results, as shown in Fig. 3. Due to its simplicity and good correlation between experimental and numerical results for the present material in this deformation range, Mooney–Rivlin constitutive law was selected for the following parametric analysis.

3. Experimental analysis of the shell under axial tension and increasing pressure

In order to understand and check the general behavior and accuracy of the parametric analysis presented herein, the experimental analysis of the shell initially stressed and submitted to increasing pressure is carried out. The results for shell B210 ($R/H = 2.63$, $L/R = 34$—see Table 1) are shown in Figs. 4–6, for increasing values of initial axial extension $\Delta L/L$. In Fig. 4, for $\Delta L/L = 0$ (shell initially unstressed), as the pressure increases, the shell deflects laterally as a long imperfect column until it reaches a critical pressure and a bubble forms nearly in the middle of the specimen. At this critical point there is a sudden drop in pressure, from 13.0×10^{-2} MPa (P_{cr}) to 7.0×10^{-2} MPa (P_{final}), indicating the existence of a limit point instability. However, the position of the bubble, which, theoretically, should be in the middle of the shell, may differ from one specimen to another. This is probably due to the effects of initial material and geometric imperfections.

3.1. Initial axial tension effects

When the shell is initially under a given axial tension, the global buckling mode is no longer observed and the shell remains in a vertical axi-symmetric configuration until it reaches the critical point, as shown in Figs. 5 and 6 for increasing axial tension. Again the shell reaches a limit point characterized by the formation of a bubble followed

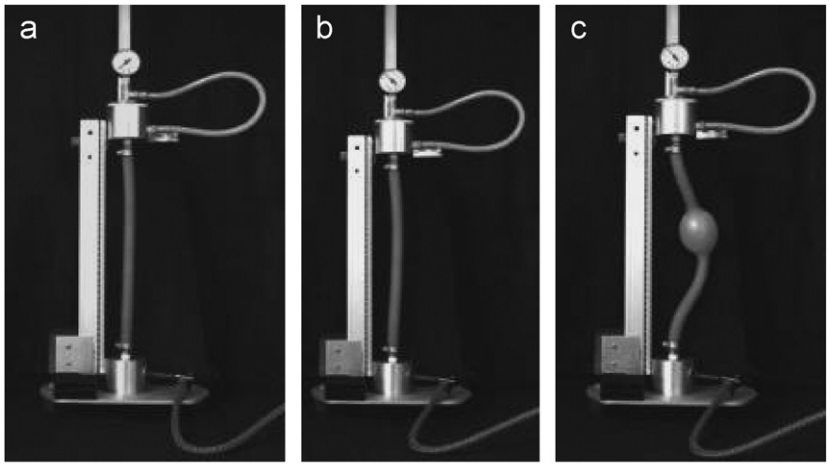

Fig. 4. Experimental analysis of an initially unstressed thick cylindrical shell under increasing internal pressure. Specimen B210. Pressure, P, in (10^{-2} MPa). (a) Initial configuration, (b) $P = 7.0$ and (c) post-critical configuration, $R/H = 2.63$, $L/R = 34$.

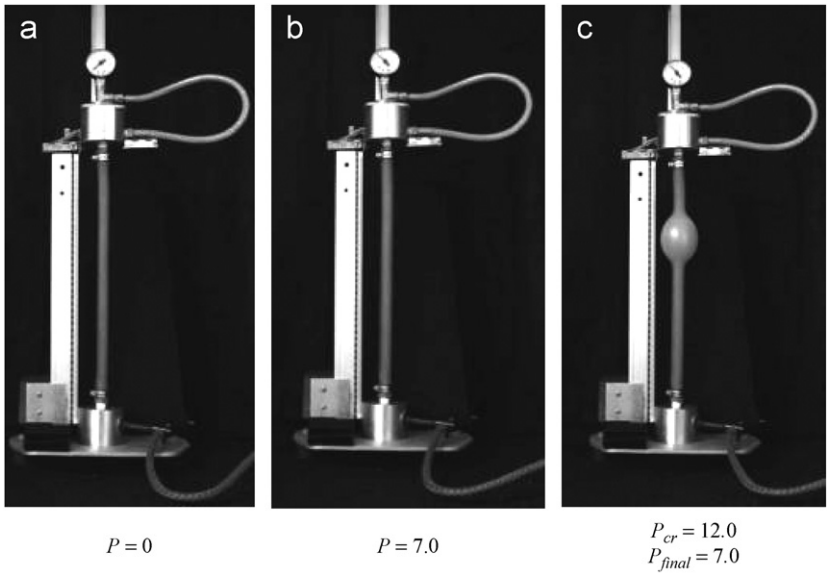

Fig. 5. Sequence of equilibrium configurations. Shell under constant axial tension, $\Delta L/L = 0.16$, and increasing internal pressure. Specimen B210. Pressure, P, in (10^{-2} MPa). (a) Initial configuration, (b) $P = 7.0$ and (c) post-critical configuration. $R/H = 2.63$, $L/R = 34$.

by a sudden drop in the internal pressure. However, a decrease in the critical load, P_{cr}, from 13.0 to 11.4×10^{-2} MPa is observed as the initial extension ratio $\Delta L/L$ increases from 0 to 0.32. On the other hand, the final pressure after the onset of the unstable buckling (P_{final}) remains practically the same, 7.0×10^{-2} MPa.

In order to understand the influence of the geometric parameters and initial axial tension on the experimental results, several tests were carried out for the shell geometries shown in Table 1. Figs. 7–9 illustrate the behavior of shells B204, B205 and B207, respectively. Each figure shows the initial and critical states of the shell for increasing values of the initial axial tension. In each case, the global behavior is similar to the one observed previously for shell B210. In all cases, the critical pressure decreases with the initial axial tension. However, the bubble localization for the same specimen may vary with the value of $\Delta L/L$, as observed in Figs. 7–9. The variation of the experimental critical load with the initial axial tension is illustrated in Fig. 10 for five shell specimens, where the value of the ratio R/H is shown in inset for each specimen. The results of this parametric analysis show that the critical load decreases with the radius to thickness ratio. This is better observed in Fig. 11 where the critical load is plotted as a function of R/H for three different values of $\Delta L/L$.

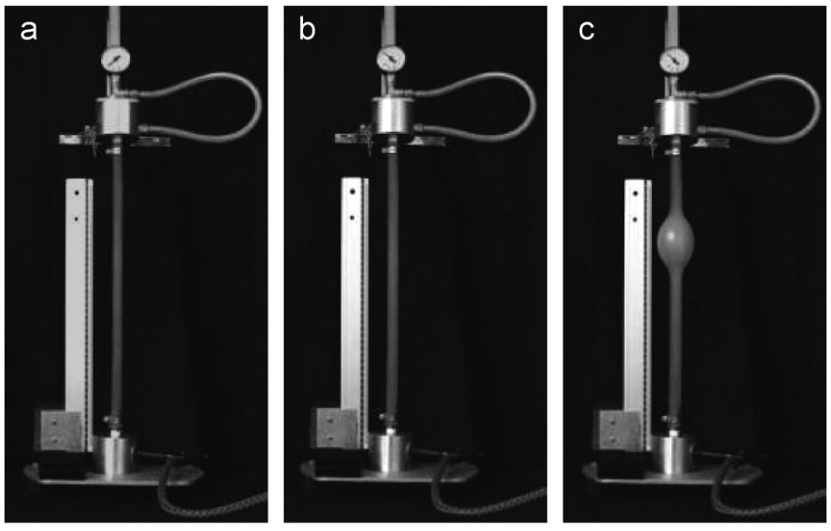

Fig. 6. Sequence of equilibrium configurations. Shell under constant axial tension, $\Delta L/L = 0.32$, and increasing internal pressure. Specimen B210. Pressure, P, in (10^{-2} MPa). (a) Initial configuration, (b) $P = 7.0$ and (c) post-critical configuration. $R/H = 2.63$, $L/R = 34$.

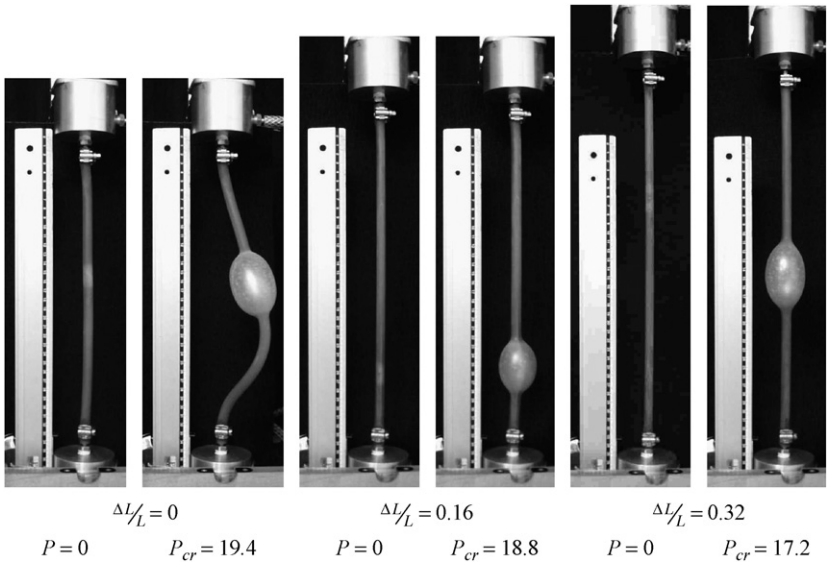

Fig. 7. Recorded equilibrium configurations for specimen B204. Pressure, P, in (10^{-2} MPa).

A short shell with a much smaller diameter (shell B200: $D = 4.84$ mm, $H = 1.22$ mm, $L = 80$ mm, $R/H = 2.0$, $L/R = 34$) was also analyzed. Fig. 12 illustrates the behavior of the initially unstressed shell for increasing pressure. The same global behavior shown previously for the other shells is observed. Again at the critical point the shell deflects laterally like a column as the bubble appears. However, for this geometry (shorter shell), the bubble extends over the entire length of the shell. The results for the same shell under increasing initial axial tension are shown in Fig. 13. For this shell specimen the bubble or aneurysm appeared near the lower support. This seems to be due the local disturbances caused by the air injector that had a diameter slightly higher than the inner diameter of this tube. This illustrates the importance of local imperfection on the bubble localization. In the present case the length of the bubble just after the onset of buckling decreases with increasing initial axial tension. More details of the experimental analysis can be found in Xavier [36].

4. Numerical results—stability analysis

In order to understand the nonlinear behavior of the shell and reproduce numerically the overall behavior observed in the experimental analysis, a detailed parametric analysis of the inflation of the extended thick tube is carried out using the FE software ABAQUS. The shell element S4R is used to discretize the shell and Riks

Fig. 8. Recorded equilibrium configurations for specimen B205. Pressure, P, in (10^{-2} MPa).

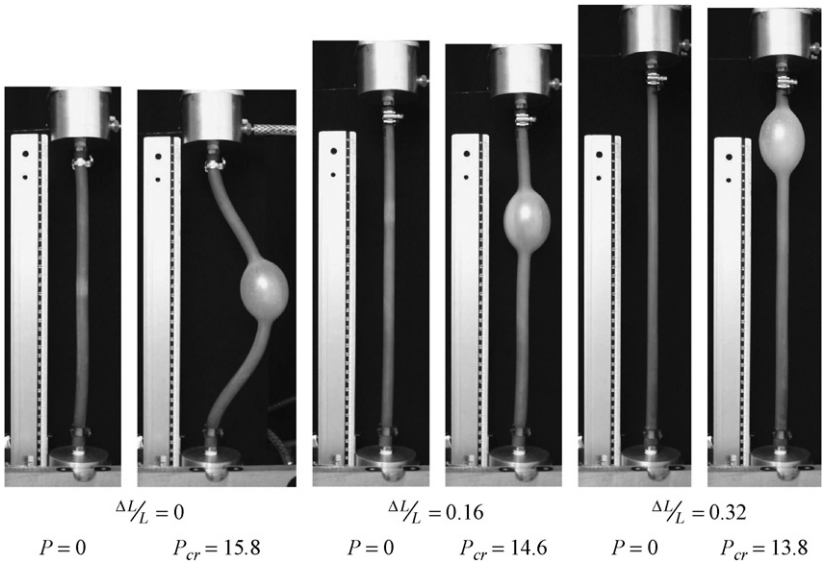

Fig. 9. Recorded equilibrium configurations for specimen B207. Pressure, P, in (10^{-2} MPa).

modified method is employed to obtain the nonlinear equilibrium path. First, a convergence study was carried out to obtain the best mesh and number of elements.

Fig. 14 illustrates the numerical results for initial and critical configurations for shell B210 with $\Delta L/L = 0.16$. A mesh with 1230 nodes and 1215 elements was used in this analysis. The critical pressure obtained numerically, 11.88×10^{-2} MPa, was 95% of the experimental one, 12.0×10^{-2} MPa. On comparing with Fig. 5, a good agreement between the numerical and experimental results can be observed.

Now the influence of the shell geometric parameters on the nonlinear equilibrium path and critical load of the shell is analyzed. First, the influence of the shell thickness is studied. Here a shell with $\Delta L/L = 0.16$, $L = 317$ mm and $R = 9.33$ mm is considered and the thickness varies from 1.0 to 3.58 mm. The nonlinear equilibrium paths are shown in Fig. 15 where the internal pressure is plotted as a function of the maximum radial displacement, U_{rmax}. Initially the tube response is relatively stiff and almost linear. As the pressure increases the shell stiffness decreases and a limit point is reached after which the internal pressure decreases as the maximum radius increases, reaching a local minimum. In a pressure-controlled experiment the descending post-critical path is unstable. This is in agreement with the experimental results where, during inflation, the tube experienced a sudden expansion which was followed by a corresponding decrease in the internal pressure due to the sudden increase in internal volume, reaching a lower bound pressure associated with

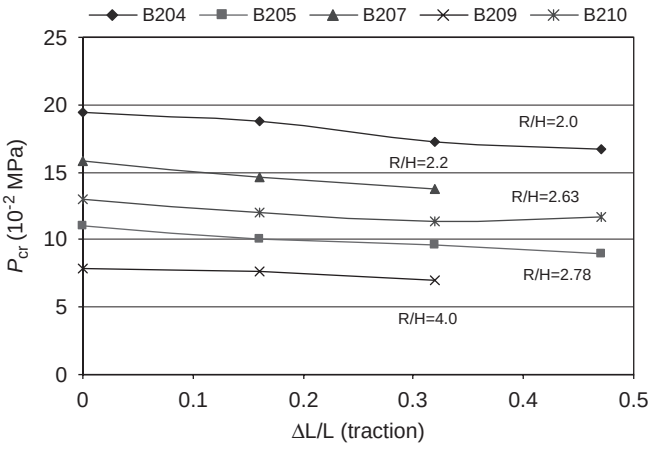

Fig. 10. Experimental results. Variation of the critical pressure as a function of the initial extension ratio, $\Delta L/L$, for several geometries.

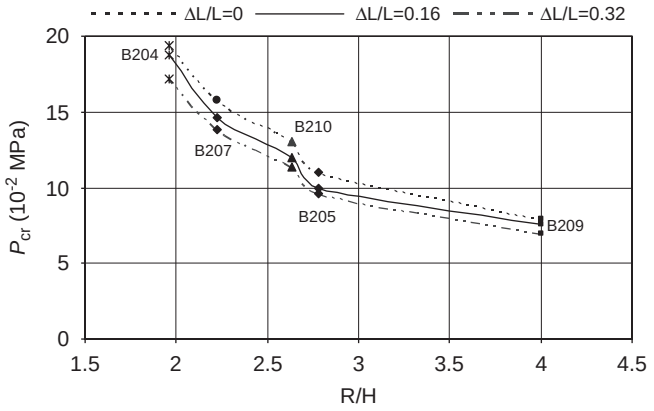

Fig. 11. Experimental results. Variation of the critical pressure as a function of the R/H ratio for three different values of the initial extension ratio, $\Delta L/L$.

large deformations. This behavior is known in literature as localization [33]. It was first predicted by Mallock [34] and observed in thick hyperelastic membranes by, among others, Kyriakides and Chang [27,28]. Also shown in Fig. 15 are the experimental values obtained for P_{cr} and P_{final} obtained for shell B210, which agree quite well with the numerical results. This behavior is typical of a softening, imperfection sensitive system. The results in Fig. 15 also show that, as the shell thickness increases (R/H decreases), i.e. H increases, the stiffness of the shell increases, increasing the critical load. This is also in agreement with the experimental results reported in Fig. 12. Fig. 16 shows a comparison of the nonlinear equilibrium path for shell B207, $L = 317$ mm and $\Delta L/L = 0.16$, with the experimental results obtained for P_{cr} and P_{final}. Excellent agreement is observed not only for the value of the critical load but also for the corresponding maximum radial deformation, which occurs in the middle of the bubble.

The influence of the shell radius on its nonlinear behavior is now analyzed, considering a shell with

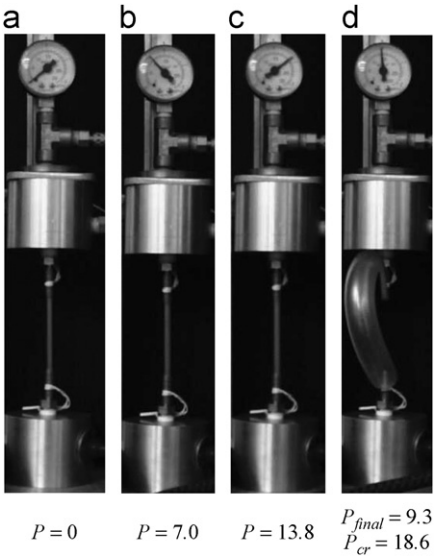

Fig. 12. Selected equilibrium configurations of an unstressed cylindrical short shell under increasing pressure. Specimen B200. Pressure, P, in (10^{-2} MPa). (a) Initial configuration, (b) $P = 7.0$, (c) $P = 13.8$ and (d) post-critical configuration.

$\Delta L/L = 0.16$, $L/L = 200$ mm and $H = 2$ mm. The shell radius varies from 3.0 to 10.0 mm. The shell nonlinear equilibrium paths are shown in Fig. 17 for different values of R, where a load–displacement response similar to that shown in Fig. 15 is observed. The variation of the critical load as a function of the shell external radius is illustrated in Fig. 18, for $\Delta L/L = 0.16$, $L = 200$ mm and $H = 2.0$ mm. There is a sharp decrease in the critical load as the radius increases. For an increase of 30% in the shell external radius, there is a decrease of 34% in the critical pressure.

The influence of the shell initial length on its nonlinear behavior is now analyzed, considering a shell with $\Delta L/L = 0.16$, $R = 5.5$ mm, $H = 2$ mm ($R/H = 2.75$) and L varying from 50 to 200 mm. The results of this parametric analysis are shown in Figs. 19 and 20. As the initial length of the tube increases, the critical load increases, approaching asymptotically a maximum value. This means that, as the length increases, the two portions of the tube away from the bubble have little effect on the onset of instability, as illustrated in Fig. 21.

The numerical results also show that the localization and number of bubbles may vary depending on the system parameters and imperfections. The imperfection sensitivity analysis and long-term behavior of the stressed thick shell are currently being analyzed.

5. Conclusions

In this work the finite deformations of a thick isotropic circular cylindrical shell subjected to a finite extension and gradually filled with air are investigated both numerically and experimentally. Theoretical and, particularly, experimental investigations of thick shells under variable pressure

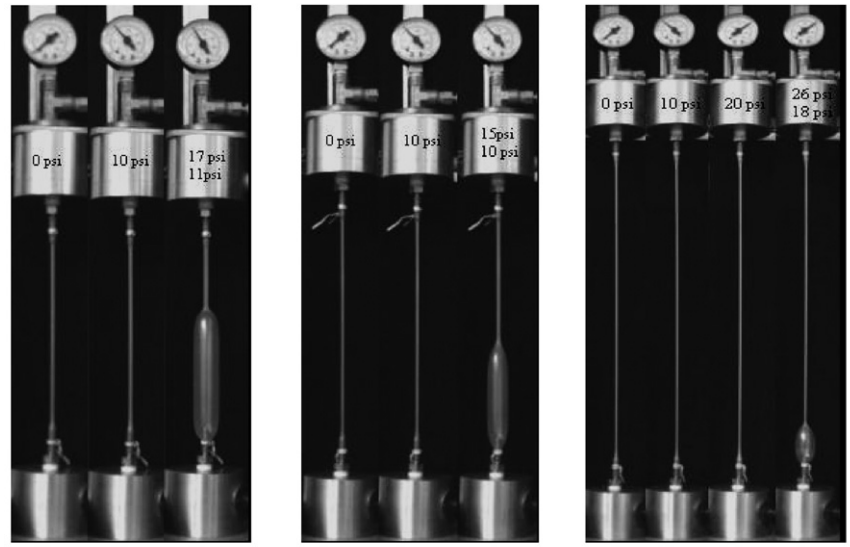

$\Delta L/L = 1.25$ $\Delta L/L = 1.87$ $\Delta L/L = 3.75$

$P = 0$ $P = 7.0$ $P_{cr} = 11.7$, $P_{final} = 7.6$ $P = 0$ $P = 7.0$ $P_{cr} = 10.3$, $P_{final} = 7.0$ $P = 0$ $P = 7.0$ $P = 13.8$ $P_{cr} = 17.9$, $P_{final} = 12.0$

Fig. 13. Recorded equilibrium configurations for specimen B200 under increasing axial tension. Pressure, P, in (10^{-2} MPa).

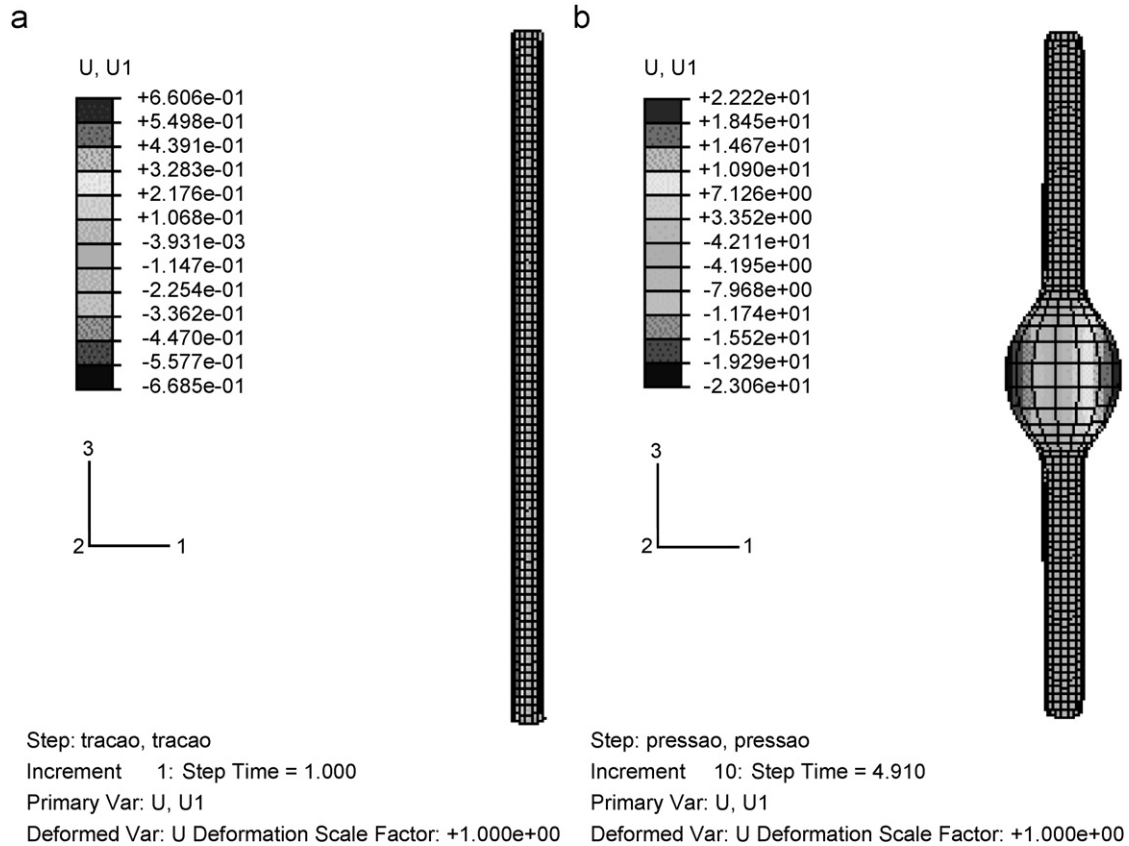

Fig. 14. Numerically obtained deformation pattern for specimen B210 with $\Delta L/L = 0.16$. (a) $P = 0$, initial equilibrium configuration, shell under axial tension, (b) $P_{cr} = 11.88$, post-critical configuration ($P \times 10^{-2}$ MPa).

and axial tension are scarce in the literature. Nonetheless, this is a problem of importance in many engineering fields, including some relevant biomedical problems. The agreement of the experimental and numerical results, especially for relatively low values of the extension ratio $\Delta L/L$, is rather encouraging and indicates that the present

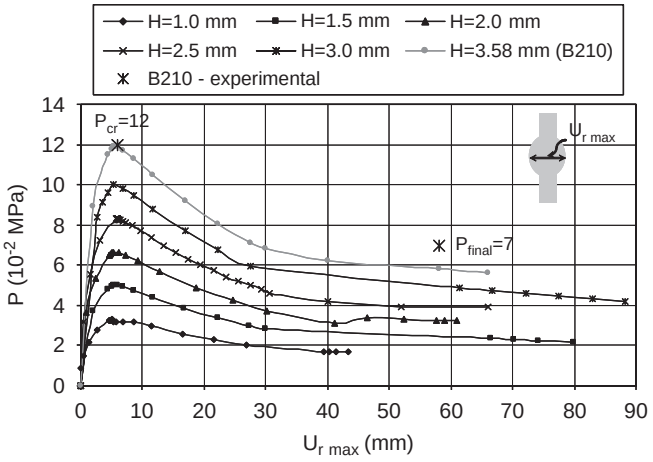

Fig. 15. Influence of the shell thickness on the nonlinear load–displacement relation for a shell with $L = 317\,\text{mm}$, $R = 9{,}33\,\text{mm}$ and $\Delta L/L = 0.16$.

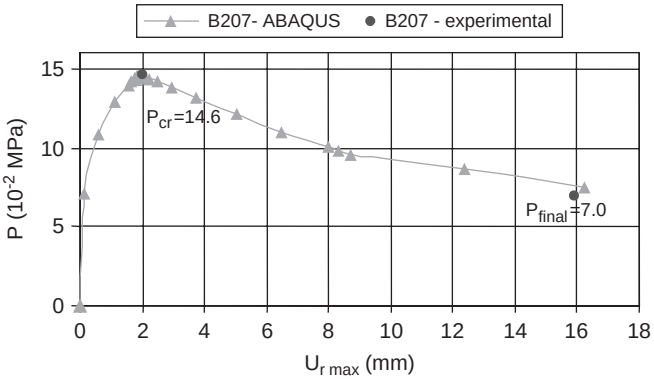

Fig. 16. Comparison between numerical and experimental results for shell B207. $L = 317\,\text{mm}$ and $\Delta L/L = 0.16$.

formulation can satisfactorily model the deformation field under consideration. Also, the experimental results presented here, covering a large collection of cases, can be used as a benchmark for future theoretical and numerical works in this area. For shell under initial axial tension, the local instability phenomenon (localization) was observed during the experiments and parametric numerical analysis: at a certain load level the shell loses its stability forming a local bubble along its length. This type of buckling mode is a characteristic of thick shells under internal pressure and may explain certain instability phenomena as localized buckling in tubes and aneurysms. For shells without initial axial tension, a more complex instability mode is observed. First, the shell deflects laterally as a long imperfect column until it reaches a critical pressure and a bubble forms nearly in the middle of the specimen. The critical pressure is a function of the shell geometry and initial axial tension.

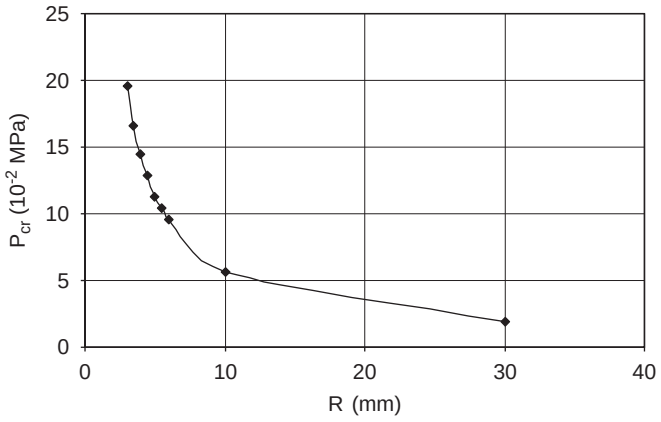

Fig. 18. Influence of the undeformed radius on the shell critical load. $L = 200\,\text{mm}$, $\Delta L/L = 0.16$ and $H = 2.0\,\text{mm}$.

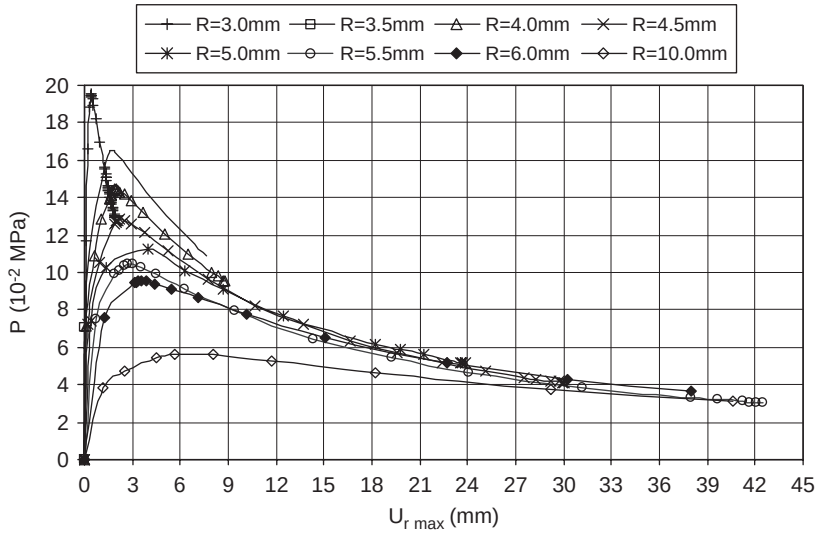

Fig. 17. Influence of the shell radius on the nonlinear load–displacement relation. $L = 200\,\text{mm}$, $\Delta L/L = 0.16$ and $H = 2.0\,\text{mm}$.

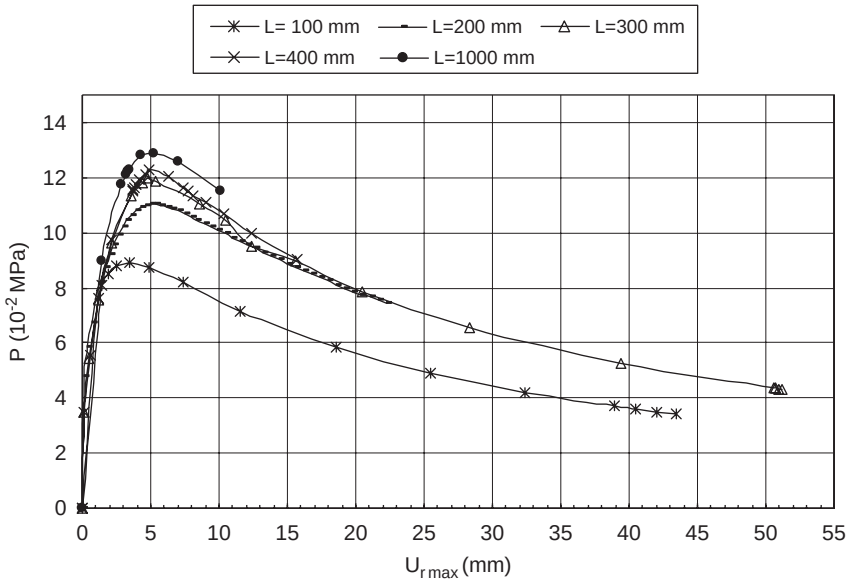

Fig. 19. Influence of the shell initial length on the nonlinear load–displacement relation. R = 5.5 mm, $H = 2.0$ mm and $\Delta L/L = 0.16$.

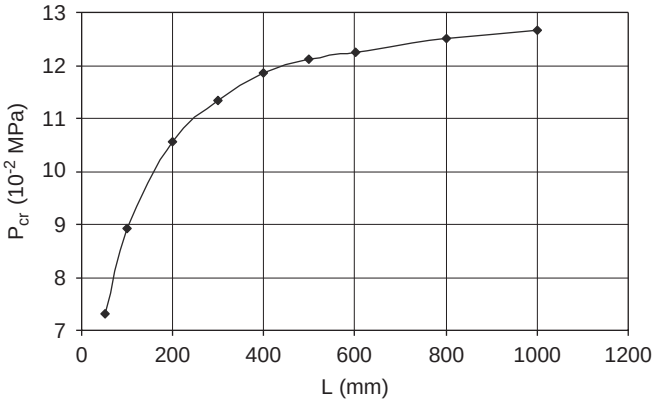

Fig. 20. Influence of the initial length L on the shell critical load.

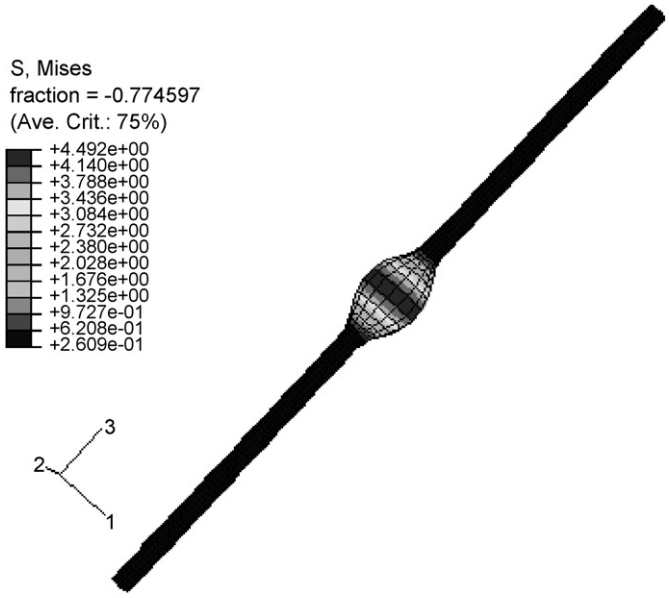

Fig. 21. Post-buckling deformation of a hyperelastic thick shell with undeformed radius $R = 3.0$ mm.

Acknowledgments

The authors are grateful to the Brazilian governmental agencies CNPq, CAPES and FAPERJ for their financial support and to one of the referees for valuables suggestions.

References

[1] Rivlin RS. Large elastic deformations of isotropic materials. Philosophical Transactions of the Royal Society A 1948;240:459–91.

[2] Barenblatt GI, Joseph DD, editors. Collected papers of RS Rivlin, vols. I and II. Berlin: Springer; 1996.

[3] Truesdell C. On the mechanical foundations of elasticity and fluid dynamics. Journal of Rational Mechanics and Analysis 1952;1:125–300.

[4] Green AE, Adkins JE. Large elastic deformations and non-linear continuum mechanics. Oxford, UK: Oxford University Press; 1960.

[5] Charlton DJ, Yang J, The KK. A review of methods to characterize rubber elastic behavior for use in finite-element analysis. Rubber Chemistry and Technology 1994;67(3):481–503.

[6] Mooney M. A theory of large elastic deformations. Journal of Applied Physics 1940;11:582–92.

[7] Rivlin RS. Large elastic deformations of isotropic materials: I. Fundamental concepts. II. Some uniqueness theorems for pure homogeneous deformation. Philosophical Transactions of the Royal Society A 1948;240:459–508.

[8] Gent AN. Elastic instabilities in rubber. International Journal of Non-Linear Mechanics 2005;40:165–75.

[9] Hart-Smith LJ. Elasticity parameters for finite deformations of rubber-like materials. Zeitschrift Fur Angewandte Mathematik Und Physik 1966;17:608–26.

[10] Alexander H. A constitutive relation for rubber-like materials. International Journal of Engineering Sciences 1968;6:549–63.

[11] Arruda EM, Boyce MC. A three-dimensional constitutive model for the large stretch behavior of rubber elastic materials. Journal of Mechanics and Physics of Solids 1993;41(2):389–412.

[12] Ogden RW. Large deformation isotropic elasticity on the correlation of theory and experiment for incompressible rubber-like solids. Proceedings of the Royal Society of London A 1972;326:565–84.

[13] Ogden RW. Non-linear elastic deformations. Chichester, UK: Ellis Horwood Ltd.; 1984.
[14] Corneliussen AH, Shield RT. Finite deformation of elastic membranes with application to the stability of an inflated and extended tube. Archive for Rational Mechanics and Analysis. 1961;1: 273–304.
[15] Alexander H. Tensile instability of initially spherical balloons. International Journal of Engineering Sciences 1971;9:151–62.
[16] Haughton DM, Ogden RW. Bifurcation of inflated circular cylinders of elastic material under axial loading—I. Membrane theory for thin-walled tubes. Journal of the Mechanics and Physics of Solids, 1979;27(3):179–212.
[17] Haughton DM, Ogden RW. Bifurcation of inflated circular cylinders of elastic material under axial loading—II. Exact theory for thick-walled tubes. Journal of the Mechanics and Physics of Solids 1979;27(5–6):489–512.
[18] Ratner AM. Tensile stability of cylindrical membranes. International Journal of Non-Linear Mechanics 1983;18:133–47.
[19] Li X, Steigmann DJ. Finite plane twist of an annular membrane. Quarterly Journal of Mechanics and Applied Mathematics 1993; 46:601–26.
[20] Haseganu EM, Steigmann DJ. Theoretical flexure of a pressurized cylindrical membrane. International Journal of Solids and Structures 1994;31:27–50.
[21] Chen Y. Stability and bifurcation of inflated cylindrical elastic membranes. In: Godoy LA, Idelshon SR, Laura PAA, Mook DT, editors. Applied mechanics in the Americas, vol. 1, 1995, p. 404–9.
[22] Haughton DM. Axially elastic membranes subjected to fluid loads. IMA Journal of Applied Mathematics 1996;56:303–20.
[23] Gent AN. Elastic instabilities of inflated rubber shells. Rubber Chemistry and Technology 1999;72(2):263–8.
[24] Pamplona D, Bevilacqua L. Large deformations under axial force and moment load of initially flat membranes. International Journal of Non-Linear Mechanics 1992;27:639–50.
[25] Pamplona D, Gonçalves PB, Davidovich M, Weber HI. Finite axisymmetric deformations of an initially stressed fluid-filled cylindrical membrane. International Journal of Solids and Structures 2001;38:2033–47.
[26] Pamplona D, Gonçalves PB, Lopes SRX. Finite deformations of cylindrical membranes under internal pressure. International Journal of Mechanical Sciences 2006;48(6):683–96.
[27] Kyriakides S, Chang YC. On the inflation of a long elastic tube in the presence of axial load. International Journal of Solids and Structures 1990;26(9–10):975–91.
[28] Kyriakides S, Chang YC. The initiation and propagation of a localized instability in an inflated elastic tube. International Journal of Solids and Structures 1991;27(9):1085–111.
[29] Tang D, Chung Y, Huang Y, Ku DN. Wall stress and strain analysis using a three-dimensional thick-wall model with fluid–structure interactions for blood flow in carotid arteries with stenoses. Computers and Structures 1999;72:341–56.
[30] Haussy B, Ganghoffer J. An orthotropic hyperelastic model of cylindrical thick shells under pressure: application to the modeling of aneurysm. In: Proceedings of the 15th ASCE engineering mechanics conference, New York, 2002.
[31] Hibbit D, Karlsson B, Sorensen P. ABAQUS standard user's manual. Version 6.2, 2001.
[32] Hibbit D, Karlsson B, Sorensen P. ABAQUS standard theory manual. Version 6.2. 2001, p. 3.6.6-1, 3.3.6-28.
[33] Tvergaard V, Needleman A. On the localization of buckling patterns. ASME Journal of Applied Mechanics 1980;47:613–9.
[34] Mallock A. Proceedings of the Royal Society of London 1890–1891;49:458–63.
[35] Treolar LRG. The physics of rubber elasticity. UK: Oxford University Press; 1975.
[36] Xavier SR. Nonlinear behavior and instabilities of hyperelastic membranes and shells. PhD dissertation, Civil Engineering Department, Pontifical Catholic University, PUC–Rio, Rio de Janeiro, Brazil, 2003.
[37] Vangenko H, Treolar LRG. The inflation and extension of rubber tube for biaxial strain studies. Journal of Physics D: Applied Physics 1978;11:1969–78.